Magnetic polarizability of octet baryons near the physical quark-mass point

Thomas Kabelitz, Waseem Kamleh, and Derek Leinweber

Special Research Centre for the Subatomic Structure of Matter (CSSM), Department of Physics, University of Adelaide, Adelaide, South Australia 5005, Australia

(Received 28 December 2024; revised 15 June 2025; accepted 25 June 2025; published 31 July 2025)

The magnetic polarizabilities of octet baryons are examined close to the physical quark-mass point using the background-field method in lattice QCD. For the first time, quantitative evidence of a light-quark exceptional configuration problem is presented. This exploratory calculation shows how these exceptional configurations have hindered previous attempts to determine magnetic polarizabilities near the physical mass point. The origin of the exceptional configuration problem lies in the use of a Wilson-type fermion action on electroquenched gauge-field configurations, where the dynamical-fermion gauge-field generation algorithm ignores the electric charges of the quarks. Changes in the fermion determinant that would suppress some gauge fields in the background magnetic field are neglected, leaving improbable gauge fields that generate large additive mass renormalizations which manifest as significant outliers in correlation-function distributions. The nature and extent of the exceptional configuration problem is illustrated through the development of an algorithm for the systematic identification and removal of the exceptional configurations. We find the light up and down quarks to be problematic, especially the up quark with its larger electric charge. The heavier mass of the strange quark protects the hyperon correlation functions to some extent. However, these also show some change upon the removal of exceptional configurations. Upon removing exceptional configurations, we find our results to be in accord with the behavior anticipated by chiral perturbation theory. However, we emphasize that there is no first-principles justification for the removal of exceptional configurations and, in light of the severity of the problem, we recommend the alternative formalism offered through the consideration of four-point function methods.

DOI: 10.1103/38db-ml51

I. INTRODUCTION

The uniform background magnetic-field formalism has been effective in enabling precision lattice QCD calculations of hadron magnetic moments and magnetic polarizabilities. By measuring the change in the energy of the hadron as a function of the background-field strength, one can extract these quantities with uncertainties that compete favorably with experimental measurements.

However, calculations of the magnetic polarizability using this approach [1–5] have previously been unable to probe the light near-physical quark-mass regime due to large and uncontrolled statistical uncertainties that appear in lattice two-point correlation functions at finite magnetic field. Statistical distributions do not respond to increases in the number of samples in the expected manner, indicating an important systematic error.

To make contact with experiment, chiral effective field theory has been used to extrapolate lattice calculations from larger unphysical quark masses to the physical point. At light-quark masses, significant chiral nonanalytic behavior is predicted. Whether this behavior is observed in lattice QCD calculations remains to be determined.

In this work, we present the first quantitative evidence of an exceptional configuration problem encountered at near-physical quark masses in nontrivial uniform background magnetic fields. The origin of the exceptional configuration problem lies in the use of a Wilson-type fermion action on electroquenched gauge-field configurations. Here, the dynamical-fermion gauge-field generation is performed at zero magnetic field, effectively neutralizing the electric charges of the quarks. In other words, the sea quarks are blind to the background magnetic field. Changes in the fermion determinant that would suppress some gauge fields are neglected. These improbable gauge fields can generate large additive mass renormalizations which manifest as significant outliers in correlation-function distributions.

We show how these exceptional configurations render the extraction of signal for nucleons impossible. While the heavier strange quarks present in the hyperons allows the

Published by the American Physical Society under the terms of the Creative Commons Attribution 4.0 International license. Further distribution of this work must maintain attribution to the author(s) and the published article's title, journal citation, and DOI. Funded by SCOAP³.

extraction of some signal, the exceptional configurations in the light sector do impact the quality of that signal.

Our main focus is to understand the nature and extent of the exceptional configuration problem through the development and testing of algorithms designed to identify these exceptional configurations and remove them from lattice QCD correlation functions. Eventually this process admits a high statistics calculation of the magnetic polarizability of ground-state octet baryons at near-physical quark masses on the lightest PACS-CS ensemble [6]. We utilize the background-field method and calculate the magnetic polarizability through a combination of spin-field aligned and antialigned two-point correlation functions. As the Λ and Σ^0 baryons mix in the background field, we consider the outer octet baryons composed of a doubly represented quark flavor and a singly represented quark flavor.

Because there is no first-principles justification for the removal of exceptional configurations, one should not regard this as a method to perform first-principles calculations. Rather it is a method that illustrates the severity of the exceptional configuration problem and the results can inform future approaches. In light of the severity of the problem revealed in the following analysis, we conclude by recommending an alternative formalism offered through the consideration of four-point function methods [7–11].

In Sec. II we briefly discuss the setup of the calculation and the simulation details are briefly reviewed in Sec. III. The exceptional configuration problem is investigated in Sec. IV, where algorithms for the systematic identification and removal of exceptional configurations are created and implemented. Animations showing the evolution of lattice correlation functions as exceptional configurations are eliminated are presented in Supplemental Material [12]. Following the removal of exceptional configurations, octet-baryon magnetic polarizabilities are calculated at the lightest PACS-CS quark mass with $m_\pi = 156$ MeV and presented in Sec. V. Drawing on our previous results at larger quark masses in Ref. [5], chiral extrapolations are performed in Sec. VI and compared with our new results to evaluate the chiral behavior observed in lattice QCD. Finally, a summary of our findings is presented in Sec. VII where we discuss the severity of the exceptional configuration problem and propose alternative approaches for both short and longer term analysis scenarios.

II. CALCULATION SETUP

Our approach to the extraction of the baryon magnetic polarizability follows our approach in Ref. [5]. In this section, we briefly review the approach drawing on the succinct summary presented in Ref. [13] exploring the quark-mass dependence of baryon magnetic polarizabilities. Full details are available in Ref. [5].

In the uniform background-field method, a minimal coupling to the discretized covariant derivative results in the application of a phase to the QCD gauge field. Through the requirement for periodicity at the two boundaries orthogonal to the magnetic-field direction, a quantization condition is obtained for the magnetic-field strength B, given by

$$eB = \frac{2\pi}{N_x N_y a^2}\frac{1}{q_d}k_d, \tag{1}$$

where k_d is an integer specifying the field strength in multiples of the minimum uniform field strength quantum. The condition is written in terms of the down quark charge $q_d e$, the number of spatial sites N_x, N_y and the lattice spacing a.

The magnetic field is defined such that the field corresponding to integer $k_d = 1$ is oriented in the negative $\hat{z}$ direction. This work utilizes quark propagators and baryon correlation functions calculated at $k_d = 0, \pm 1, \pm 2$. We will refer to the strength of the magnetic field in terms of k_d throughout this work.

This uniform background magnetic field imparts a change in the energy of the baryon as a function of magnetic field strength [14,15]

$$E(B) = m + \vec{\mu}\cdot\vec{B} + \frac{|q_B eB|}{2m}(n+1) - \frac{1}{2}4\pi\beta B^2 + \mathcal{O}(B^3). \tag{2}$$

Here contributions from the magnetic moment $\vec{\mu}$ and the magnetic polarizability β complement the mass of the baryon m. The third term of Eq. (2) provides the Landau-level contribution proportional to $|q_B eB|$ where q_B is the charge of the baryon. We use a U(1) Landau-mode projection [3] to select $n = 0$.

The sign of the magnetic moment term is dependent on the alignment of the baryon's spin and the magnetic field. As such, it may be eliminated through summation of a "spin-field aligned" correlation function $G_{\uparrow\uparrow}(B)$ and a "spin-field antialigned" correlation function $G_{\uparrow\downarrow}(B)$.

The effective energy of the correlation-function ratio

$$R(B,t) = \frac{G_{\uparrow\uparrow}(B,t)G_{\uparrow\downarrow}(B,t)}{G(0,t)^2} \tag{3}$$

subtracts the magnetic moment term and the contribution from the baryon mass leaving the magnetic polarizability energy shift $\delta E_\beta(B,t)$,

$$\delta E_\beta(B,t) = \frac{1}{2}\frac{1}{\delta t}\lim_{t\to\infty}\log\left(\frac{R(B,t)}{R(B,t+\delta t)}\right), \tag{4}$$

$$= \frac{|qeB|}{2m} - \frac{4\pi}{2}\beta|B|^2 + \mathcal{O}(B^3). \tag{5}$$

As the construction of the ratio $R(B,t)$ aggregates the positive and negative magnetic-field strengths, we fit

$\delta E_\beta(B,t)$ as a function of field strength to extract the magnetic polarizability.

In practice, it is simpler to fit in terms of the field strength quanta k_d. Using the quantization condition Eq. (1), we can write the above as

$$\delta E_\beta(k_d) = L(k_d, m) + C\beta k_d^2, \tag{6}$$

where the Landau term is given by

$$L(k_d, m) = \frac{2\pi}{N_x N_y a^2}\frac{1}{2m}\left|\frac{q_B}{q_d}k_d\right|, \tag{7}$$

and the coefficient to the k_d^2 term is

$$C = -\frac{1}{2\alpha}\left[\frac{2\pi}{N_x N_y a^2}\right]^2\frac{1}{q_d^2}. \tag{8}$$

Here $\alpha = \frac{e^2}{4\pi}$ is the fine structure constant. It is important to note that q_d is the down quark charge while q_B is the hadronic charge of the baryon.

To obtain $\delta E_\beta(k_d)$ and m, we utilize a weighted average of fit windows to provide a systematic approach to fitting. We consider fit windows $[t_s, t_f]$ with minimum length three corresponding to $t_f \geq t_s + 2$ in range $[t_{\min}, t_{\max}]$. We set $t_f = t_{\max}$ to ensure equitable sampling of all time slices. $t_{\max}$ is chosen as the last time slice before signal is lost to noise. We choose $t_{\min} = 20$ as the level of available signal we have access to at the lightest PACS-CS quark mass makes it impossible to consistently satisfy the "log G" requirements we imposed at heavier quark masses in Ref. [5]. The choice of $t_{\min} = 20$ is chosen to give maximum opportunity for the excited-state contamination to ease while ensuring that we have windows of the requisite length available for sampling. The utilization of a weighted average of eligible windows enforces the sampling of later windows and this will further aid in suppressing the excited-state contamination.

In Ref. [5], we utilized a criterion which weighs the probability of the fit's χ^2 compared to its uncertainty. This weighting is appropriate when there is already confidence that all candidate windows have reached single-state isolation. As we are unable to consistently fit in such a region on this near-physical mass ensemble, we utilize a different weighting criterion. Here we use a form of the Akaike information criterion (AIC) [16] to provide a weight [17]

$$w = \exp\left(-\frac{1}{2}[\chi^2 + n_{\text{data}} - 2n_{\text{d.o.f.}}]\right), \tag{9}$$

for each fit window. This measure depends purely on the quality of the fit. This form of the AIC inherently biases later, shorter windows, further suppressing any excited-state contamination.

The weights are normalized, $\tilde{w}_i$, such that $\sum_i \tilde{w}_i = 1$. The average effective energy is then

$$E = \sum_i^n \tilde{w}_i E_i, \tag{10}$$

and the statistical error

$$(\delta E)^2 = \sum_i^n \tilde{w}_i (\delta E_i)^2. \tag{11}$$

A weighted average is also used to obtain the mass in the Landau term where required in fitting Eq. (6). As in Ref. [5], a jackknife error estimate is performed to determine the uncertainty in the magnetic polarizability.

III. SIMULATION DETAILS

The simulation details in this work are almost identical to those of our previous work [5,13], exempting Sec. III G on statistics. Here, a much greater statistical sample is required to obtain signal in correlation functions this close to the physical point.

A. Gauge ensembles

In this work we present new results on the lightest PACS-CS ensemble while drawing on our results on the four heavier PACS-CS ensembles from Ref. [5]. The ensembles are $2+1$-flavor dynamical gauge configurations provided by the PACS-CS Collaboration [6] through the International Lattice Data Grid [18]. The configurations have a range of degenerate up and down quark masses while the strange quark mass is fixed. The strange quark mass of the ensembles which corresponds to $\kappa_s = 0.13640$ does not extrapolate to the physical kaon mass [19]. Use of $\kappa_s = 0.13665$ for the valence strange quark mass produces the correct value for the kaon mass extrapolated to the physical point [20]. We note that the mass of the strange quarks in the sea remains at the heavier mass.

Each of the ensembles are a $32^3 \times 64$ lattice. The gauge action is the Iwasaki gauge action and the clover fermion action with $C_{\text{SW}} = 1.715$ is the background-field corrected clover fermion action [4], tuned to remove the nonphysical magnetic-field induced additive mass renormalization. Details of the ensembles are summarized in Table I. At the lightest quark mass holding the focus of this investigation, the spatial cubic lattice has a length $L = 3.0$ fm.

As only the valence quarks interact with the background magnetic field, the ensembles are electroquenched. While it is possible to include the background field in the process of generating each gauge-field configuration, this would require a separate Monte Carlo simulation at each field strength. Such separate simulations would remove the correlated QCD fluctuations which are otherwise efficiently removed through the ratio in Eq. (3) and vital to

TABLE I. Details of the PACS-CS ensembles used in this work. The lattice spacing of each ensemble is set using the Sommer scale with $r_0 = 0.4921(64)(+74)(-2)$ fm. In all cases $\kappa_s^{\text{sea}} = 0.13640$ and $\kappa_s^{\text{val}} = 0.13665$ [20]. N_{con} describes the number of configurations.

m_π^{PACS} (MeV)	κ_{ud}	a (fm)	N_{con}
701	0.13700	0.1022(15)	399
570	0.13727	0.1009(15)	397
411	0.13754	0.0961(13)	449
296	0.13770	0.0951(13)	399
156	0.13781	0.0933(13)	197

resolving a signal. Without this correlation, a very significant increase in statistics would be required. As including the background field in the gauge-field generation process may address the exceptional configuration problem studied here, it will be important to consider this in a next generation calculation.

B. Baryon interpolating fields

The commonly used proton interpolating field in lattice QCD is given by [21]

$$\chi_p(x) = \epsilon^{abc}[u^{aT} C\gamma_5 d^b(x)]u^c(x), \tag{12}$$

where C is the charge-conjugation matrix. The interpolating fields of the other outer octet baryons may be easily obtained through appropriate substitution of doubly and singly represented quark flavors. This is the form of the interpolating field used throughout this work.

These interpolating fields are typically used in concert with traditional gauge-covariant Gaussian smearing to improve overlap with the baryon ground-state relative to excited states. However, it is now well established that this approach is ineffective in isolating the baryon ground state in a nontrivial background field [3,5,15,22–24]. Spherical spatial symmetry is broken by the uniform background field. Landau-mode physics affects both the quark and hadronic degrees of freedom and this must be accommodated.

C. Quark operators

As detailed in Ref. [5] and succinctly summarized in Ref. [13], we utilize an asymmetric source and sink to maximize the overlap of the lowest energy baryon eigenstates in nontrivial magnetic fields. The operators take advantage of the novel spatial symmetry of Landau modes as highlighted above.

The source and sink operator construction utilizes links which have been smeared using stout link smearing [25]. We apply ten sweeps of smearing to the spatially oriented links using an isotropic smearing parameter of $\alpha_{\text{stout}} = 0.1$.

The quark source is constructed using three-dimensional, gauge-invariant Gaussian smearing [26]. $\alpha = 0.7$ is used with 250 sweeps.

The construction of our baryon source is designed to provide a representation of the QCD interactions with the intent of isolating the spherically symmetric QCD ground state. The quark-level physics, encapsulating the effects of the electromagnetic and QCD interactions, is addressed through the eigenmode projection techniques demonstrated in Ref. [3]. A comprehensive discussion of the mechanisms may be found there. A brief presentation is provided in Ref. [5].

As discussed succinctly in Ref. [13], the eigenmodes of the two-dimensional lattice Laplacian are calculated on the $\mathrm{SU}(3) \times \mathrm{U}(1)$ gauge links. These eigenmodes are used to produce a projection operator which is applied to the quark propagator at the sink. Reference [3] showed that including too few modes results in a noisy hadron correlation function. This is similar to that observed for traditional sink smearing. As a result, the number of modes is selected to be large enough to minimize the noise of the correlation function, but small enough to retain the focus on the low-energy Landau-mode physics. The investigations of Ref. [3] found that $n = 96$ modes provides a good balance between these two competing effects and we use this here.

D. Boundary conditions

For the calculation of the quark propagators, periodic boundary conditions are used in the spatial dimensions. To avoid signal contamination from the backward propagating states, we use fixed boundary conditions in the temporal direction. The source is then placed at $t = 16$, one quarter of the total time-dimension length such that one is always away from the fixed boundary by using the middle part of the lattice time dimension.

E. Hadronic projection

With the quark-level electromagnetic physics addressed by the $\mathrm{SU}(3) \times \mathrm{U}(1)$ eigenmode projection at the sink, we turn our attention to the hadronic level. Here, the inclusion of the background magnetic field changes the wave function of a charged baryon [27]. Thus the hadronic annihilation operator requires a spatial weight that reflects the appropriate electromagnetic characteristics. To ensure $n = 0$ in Eq. (2), we project the final-state charged baryons to the Landau state corresponding to the lowest-lying Landau level.

The lowest-lying Landau mode has degeneracy $n = |k_d \frac{q_B}{q_d}|$. As discussed in Ref. [5], we use a linear combination of degenerate eigenmodes providing an optimal overlap with the quark source. This hadronic eigenmode-projected correlation function offers superior isolation of the ground state as shown in Ref. [28] and is crucial for the fitting of constant plateaus in the energy shift of Eq. (5) herein.

F. Magnetic field

Baryon correlation functions are calculated for five magnetic fields corresponding to $k_d = -2, -1, 0, 1, 2$. In doing so, quark propagators and eigenmodes are calculated at $k_d = 0, \pm 1, \pm 2$, and ± 4 in accounting for the up quark. The nonzero-field strengths correspond to magnetic fields in the z direction of $eB = \pm 0.087, \pm 0.174$, and ± 0.348 GeV^2.

G. Statistics

As periodic boundary conditions are used in all four dimensions for the gauge-field generation, one can exploit the associated translational invariance of the gauge fields. A quark source can be placed at any position on the lattice and then circularly cycled to the standard source position of $(x, y, z, t) = (1, 1, 1, 16)$. This enables additional sampling of the full gauge field.

Further, the two-dimensional nature of the lattice Laplacian operator allows the eigenmodes for the sink projection to be reused when the gauge field is cycled solely in the time direction.

Hence, we increase our statistics on the PACS-CS ensembles by considering a random spatial source location at $t = 16$ and then circularly cycling in spatial dimensions to (1, 1, 1, 16). This spatial source is considered 8 times by circularly cycling the gauge field in the temporal direction by an eighth of the lattice time extent (eight slices in our case).

On the four heavier PACS-CS ensembles, we consider four random spatial source locations while on the lightest ensemble we consider 32 random source locations. These multiple samples are binned and averaged as a single configuration estimate in the error analysis. Considering random spatial sources, their cycle in time, the number of gauge fields and the consideration of five magnetic fields, this results in 250 K unique correlation functions for each baryon at the lightest PACS-CS quark mass.

IV. EXCEPTIONAL CONFIGURATIONS

Looking at the full untouched set of configurations on the lightest PACS-CS gauge ensemble, we see clear signs of unusual behavior. Figure 1 shows the difference in plateau behavior for the magnetic polarizability energy shift δE_β of Eq. (4) for the proton on the lightest PACS-CS ensemble (left) and second-lightest PACS-CS ensemble (right) labeled by $m_\pi = 156$ and 296 MeV respectively. This highly erratic behavior of the magnetic polarizability energy shift does not respond to increased statistics. As we will demonstrate, the cause of this behavior is exceptional configurations.

In this section, we begin by reviewing the origin of exceptional configurations and then describe the algorithm we have created to systematically remove them.

A. Wilson-type fermions

The computationally efficient Wilson-clover fermion action used in this work breaks global chiral symmetry, introducing an additive mass renormalization to the Dirac operator. This shifts the point where the renormalized quark mass is zero away from the point where the bare tree-level quark mass vanishes. Of course this effect is well known and the solution is to consider the pion mass as a function of the bare quark mass. One need only determine the bare quark mass where the pion mass vanishes (usually by linear extrapolation of m_π^2) and consider bare quark masses relative to this point, referred to as the critical quark mass. This principle is used in generating the $2+1$-flavor dynamical configurations considered here.

Problems arise when improbable configurations are considered. Historically, this problem was encountered in the quenched approximation to QCD. Gauge configuration probabilities that would be suppressed by the fermion determinant in full QCD were admitted to the ensemble. These improbable configurations could induce uncharacteristic additive mass renormalizations that would lead to divergent behavior.

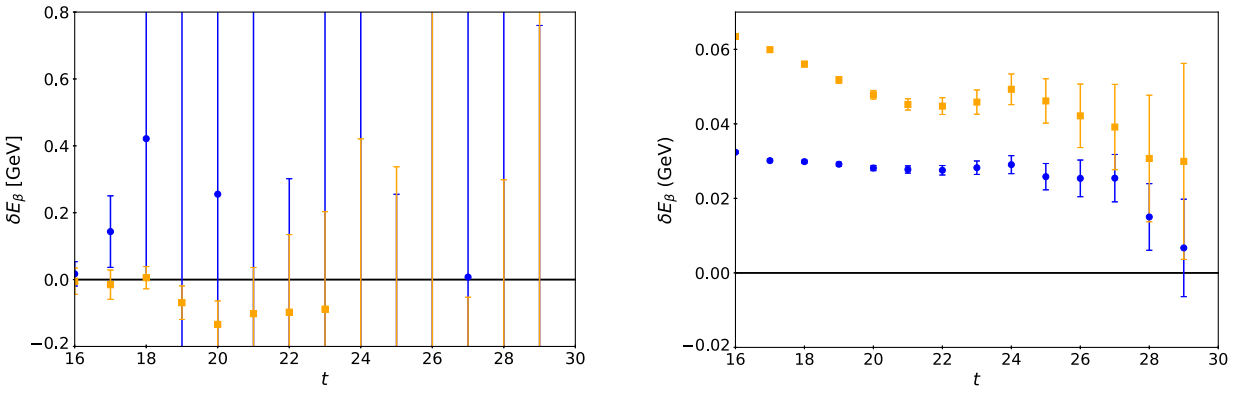


FIG. 1. The magnetic polarizability energy shift δE_β of Eq. (4) for a proton on the lightest (left) and second lightest (right) PACS-CS ensembles labeled by $m_\pi = 156$ and 296 MeV respectively. Noting the y-axis limits, we see clear signs of exceptional behavior with a wildly fluctuating plateau at the lightest mass. This is in spite of a fourfold increase in statistics.

In the generation of dynamical-fermion gauge configurations the fermion determinant acts to suppress the probability of creating configurations which give rise to approximate zero modes of the Dirac operator. In the quenched approximation, the fermion determinant is set to a constant and a proliferation of approximate zero modes is encountered. At sufficiently light renormalized quark mass, it is possible to have the critical mass realized on a particular configuration near the bare mass [29], introducing a divergence in the quark propagator. Such "exceptional" configurations provide hadronic correlation functions which differ significantly in magnitude from the average, introducing large statistical uncertainties and spoiling the ensemble average result.

In the early days of lattice QCD, when the calculation of a quark propagator would be the dominant computational cost, it was common to only consider one fermion source per gauge-field configuration. Divergent behavior was then attributed to the configuration. However, in modern simulations with several fermion sources per gauge field, it is now understood that the divergent behavior depends on both the configuration and the source position. In the following, we preserve the original terminology of an "exceptional configuration"; however, it should be understood that "configuration" refers to a particular source on a particular gauge field.

The common consideration of electroquenched configurations in the background-field formalism admits the opportunity to consider improbable gauge fields in the ensemble; these are gauge fields that would be suppressed by the fermion determinant if the dynamical sea quarks were not blind to the presence of the background magnetic field. Again, additive mass renormalization on an improbable gauge field can induce divergent behavior when the bare quark mass approaches the critical quark mass, as it does for the lightest PACS-CS ensemble.

Exceptional configurations manifest in this calculation in two ways. Rarely, the conjugate-gradient algorithm will fail to invert the Dirac operator at the required tolerance due to the singular nature of the propagator. More commonly, a fermion-matrix inversion converges providing a quark propagator with uncharacteristic behavior. As an outlier, it spoils the ensemble average and contributes to create a drastically increased uncertainty that not does respond to increased statistics.

We observe that each baryon responds differently to exceptional configurations, with the sensitivity governed by the role the propagator plays in the correlation function and the environment that it is within. We find that the inclusion of strange quarks increases the tolerance of baryon correlation functions to exceptional configurations. Nevertheless, the presence of light quarks remains problematic. Our worst case is that of the proton, where the doubly represented u quark requires the largest magnetic-field strength with $k_d = \pm 4$. Still the rate at which exceptional configurations are identified in the following, even for this worst-case example, is only 1.4%, far below the quenched occurrence of 6% for $m_\pi = 306(7)$ MeV reported in Ref. [29] using the favorable mean-field improved fat-link irrelevant clover fermion action [30].

B. Identifying exceptional configurations

Recalling that an exceptional configuration depends on both the configuration and the fermion source position, our full list of N configurations to examine is the product of the 197 gauge field configurations in the lightest PACS-CS ensemble and the full set of randomized fermion source locations. We utilize the baryon correlation function determined on small sets of these configurations as a proxy to check each configuration for exceptional behavior. Each baryon is analyzed for its unique set of exceptional configurations.

We consider a full set of N correlation functions in random order and examine a subset of M correlation functions. To determine the effective energy and associated uncertainty we:

(1) Construct a periodic list of correlation functions of length $N + M - 1$.
(2) Given the ith subset of correlation functions $\{C_i, \ldots, C_{i+M-1}\}$ determine the effective energy $E_i(t)$ and uncertainty $\Delta E_i(t)$.
(3) Repeat for $i \in [1, N]$.

We emphasize that the ith elements of $\{E_1, \cdots E_N\}$ and $\{\Delta E_1, \cdots \Delta E_N\}$ are the effective energy and associated uncertainty of the corresponding subset of correlation functions in the ith subset. We will refer to evolution of the index i as evolution in configuration time. It is also important to emphasize that these quantities are distinct from the magnetic polarizability alone as we seek a method of identifying exceptional configurations which is not tied to the final desired observable.

Figure 2 presents a plot of the uncertainty of the effective energy, $\Delta E_i(t)$, for the ith configuration subset of $M = 20$ configurations at $t = 18$, two time slices following the source at $t = 16$. We have found it is helpful to search for exceptional configurations at early time slices where the statistical fluctuations are normally small. Plotting these quantities as a function of configuration time results in an approximately constant line which exhibits sharp step function behavior whenever an exceptional configuration enters the subset of M considered configurations. The step lasts for precisely M steps in configuration time until the exceptional configuration leaves the subset.

The identification of an exceptional configurations requires identification of when these sharp changes occur. While the subensemble average also sees a step change, we find the step change in the uncertainty in the effective energy to provide a more robust indicator with greater sensitivity.

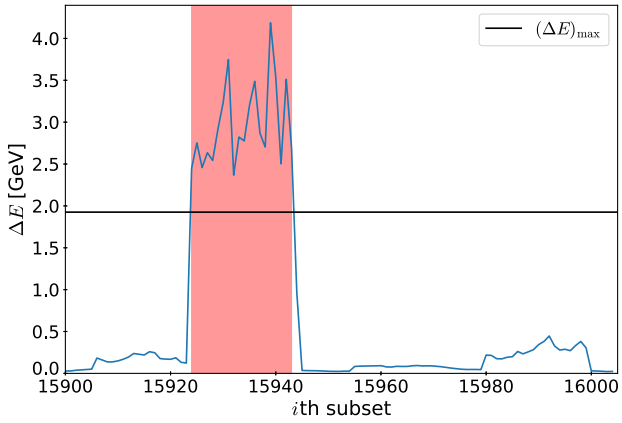


FIG. 2. The step function behavior of $\Delta E_i(t = 18)$ is illustrated as a function of configuration time for the ith subset. The jump in the uncertainty is caused by the inclusion of an outlying exceptional configuration contribution to the average over $M = 20$ configurations. The horizontal line shows the exceptional configuration identification threshold which is updated after each iteration of the algorithm as described in the text. Another exceptional configuration of smaller magnitude beginning at $i = 15980$ will be identified in a subsequent iteration.

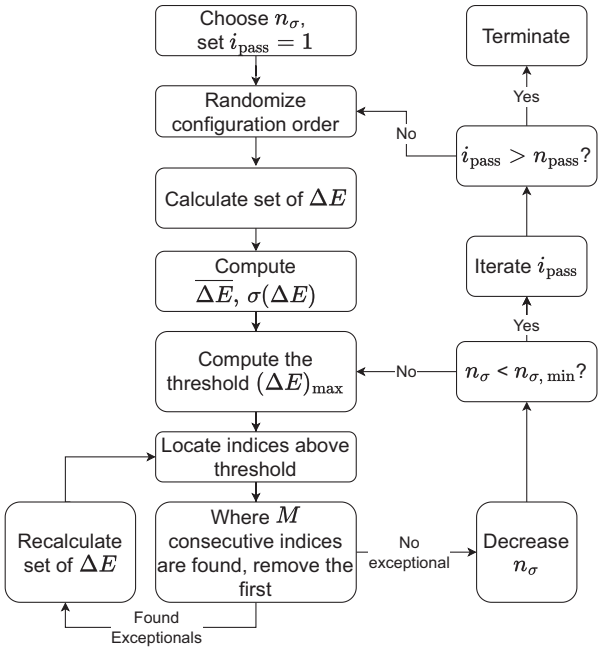


FIG. 3. Flowchart of the exceptional configuration identification algorithm described in the text.

Our algorithm, presented in detail in the following, is presented visually in Fig. 3. The algorithm runs concurrently across a range of time slices, from $t = 18$ two time slices beyond the source to where we expect to lose signal, $t = 25$. In practice, most exceptional configurations are identified at time slices close to the source as the rapidly increasing noise associated with the baryon correlation function obscures exceptional configurations at later time slices. If a configuration is found to be exceptional on any time slice, it is removed from the configuration list. Understanding that the calculations are performed concurrently at all relevant time slices, we drop the time dependence in the following discussion.

We commence by determining a threshold (corresponding to the horizontal line in Fig. 2) above which a configuration subset's energy uncertainty is considered exceptional. We consider the entire set of subensembles with uncertainties $\{\Delta E_1, \cdots \Delta E_N\}$ and calculate the mean $\overline{\Delta E}$ and standard deviation of the distribution of uncertainties, $\sigma(\Delta E)$. The threshold is set as

$$(\Delta E)_{\max} = \overline{\Delta E} + n_\sigma \sigma(\Delta E), \tag{13}$$

where n_σ is the number of standard deviations from the mean. We typically begin with $n_\sigma = 20$, a large conservative value to ensure that no exceptional configurations are found initially.

Using the threshold calculated above, we construct a list of all i subensembles where $\Delta E_i > (\Delta E)_{\max}$ and identify where we have at least M consecutive indices. In this case, the first of the consecutive indices corresponds to an exceptional configuration. We allow the number of consecutive indices to be greater than M as this allows for the removal of exceptional configurations which superpose other configurations due to being close to each other in the list.

Identified exceptional configurations are removed, triggering a recalculation of the E_i and ΔE_i. However, we do not update $(\Delta E)_{\max}$ as subsequent iterations at this point are aimed at removing exceptional configurations that overlapped within the subensembles of M configurations and therefore were not eliminated. A new list of all i subensembles where $\Delta E_i > (\Delta E)_{\max}$ is created. Again, where there are at least M consecutive indices the first index is identified as exceptional.

This process of removal, updating E_i and ΔE_i and identification of exceptional configurations, continues until no new configurations are identified as exceptional. This process ensures the algorithm is as conservative as possible.

Whenever exceptional configurations are unable to be found at the established threshold, we then decrease n_σ by a small amount and recalculate $(\Delta E)_{\max}$. In practice, we decrease n_σ by 0.1 at each step.

Our aim is to save a configuration list surviving at a target threshold $n_{\sigma,\min}$. We will run the algorithm over values of $n_{\sigma,\min}$ from 20 down to 2 with a target step size of 0.25. The fine grain and broad range allow for very precise identification of when the character of the effective energy shift plateau changes. We note that each target value starts from a different randomized ordering of the configurations and this further aids in identifying the best target value for

$n_{\sigma,\min}$ for eliminating the minimum number of exceptional configurations possible.

Thus, the algorithm continues to iterate until $n_{\sigma,\min}$ is reached. At the termination of the algorithm we save the list of configurations that have survived the criteria for the further analysis. This constitutes one pass of the algorithm.

In addition, there is some dependence in the identification of exceptional configurations on the ordering of the configurations. Upon completion of a pass, the list of remaining configurations is randomized. The value of n_σ is reset to the initial value, and the algorithm runs again. This repeats until a predetermined number of passes is completed. Here we create configuration lists for $n_{\text{pass}} \in \{2, 3, 4, 5, 6\}$.

The configuration lists for specific values of $n_{\sigma,\min}$ and n_{pass} are then sorted by the number of configurations surviving. This enables an examination of the behavior of the magnetic polarizability energy shift profile as a function of the number of exceptional configurations removed for each baryon separately. Animations are provided in Supplemental Material [12]. We find these animations to be particularly helpful in determining the minimum number of configurations to eliminate to obtain a step change in the statistical errors of the energy shift.

C. Field strength dependence of exceptional configurations

It is the inclusion of the background magnetic field which causes the presence of exceptional configurations due to the electroquenching associated with neglecting the background magnetic field in the gauge-field generation process. As a result, larger magnetic-field strengths produce greater rates of exceptional configurations. As a result, we examine the largest baryon magnitude field strengths $k_d = \pm 2$ first. For baryons with a u quark, field strengths with $k_d = \pm 4$ are included in the calculation of the baryon correlation function.

In determining the magnetic polarizability, we consider baryon spin-field aligned and antialigned orientations for each of the magnetic-field strengths. Extensive testing was done to determine the best approach for considering these spin-field orientations. We find exceptional configurations are most efficiently identified when the spin-field aligned and antialigned correlation functions are averaged for a given magnetic-field orientation, effectively averaging spin up and down baryon orientations.

Thus, baryon field strengths $k_d = 2$ and $k_d = -2$ are considered separately and we take the union of the set of exceptional configurations found for each field. We then progress to checking $k_d = \pm 1$ separately having already removed the configurations found at $k_d = \pm 2$. Checking the positive and negative field strengths separately ensures that neither field strength is unnecessarily biased. Checking the larger magnitude field strength first ensures we omit the majority of configurations which are exceptional as early as possible.

D. Summary

We emphasize that it is unnecessary to explicitly check the $k_d = 0$ correlation functions, as we do not anticipate the presence of any exceptional configurations in the zero-field case. A very small number of exceptional configurations can be found with our algorithm, but their removal has no impact on the profile of the effective energy.

As we will see in the following section reporting our results, it is not easy to define a consistent stopping criterion for when to cease removing exceptional configurations identified by our algorithm. Moreover, each of the octet baryons have different susceptibilities to exceptional configurations and require different proportions of exceptional configurations to be removed. It is here that the animations of Supplemental Material [12] are particularly helpful.

V. LATTICE RESULTS

Here we present the results for each baryon. We show the effective energy shift, $\delta E_\beta(B, t)$, of Eq. (4) for both baryon field strengths $k_d = 1$ and 2. We show the energy shift for the original case of no configurations removed and subsequently the results from the removal of the minimal number of exceptional configurations to resolve the effective energy at $k_d = 1$ and 2 respectively.

The determination of this minimal number of exceptional configurations follows from the animations of Figs. S1–S6 in Supplemental Material [12], showing the evolution of the effective energy shift as the number of exceptional configurations removed increases. The animations show that the quality of the effective energy shift does not gradually improve as configurations are removed, rather the uncertainties reduce significantly and suddenly and resolve the presence of plateau behavior. Due to the differing number of exceptional configurations observed at each field strength, the $k_d = 1$ plateau improves first, followed by the $k_d = 2$ plateau. These are the results presented in the following figures.

In Fig. 4 for the nucleons, Fig. 5 for the Σ baryons, and Fig. 6 for the Ξ baryons we show the effective energy shift in the initial state with no exceptional configurations removed on the left, after the resolution of the $k_d = 1$ plateau behavior in the middle and after the resolution of the $k_d = 2$ plateau behavior on the right. Note that the $k_d = 2$ plateau shows some improvement as the $k_d = 1$ plateau is resolved, but further exceptional configuration removal to resolve the $k_d = 2$ plateau on the right is crucial, typically extending the plateau further in Euclidean time.

In calculating the magnetic polarizability, we choose to fit the effective energy shift immediately after the $k_d = 2$ plateau resolves. As discussed earlier, we utilize the weighted averaging method discussed in Sec. II, sampling fit windows beginning at $t_{\min} = 20$ up to the point where the signal is lost which varies for each baryon. The results and $t_{\max}$ values for all baryons are summarized in Table II.

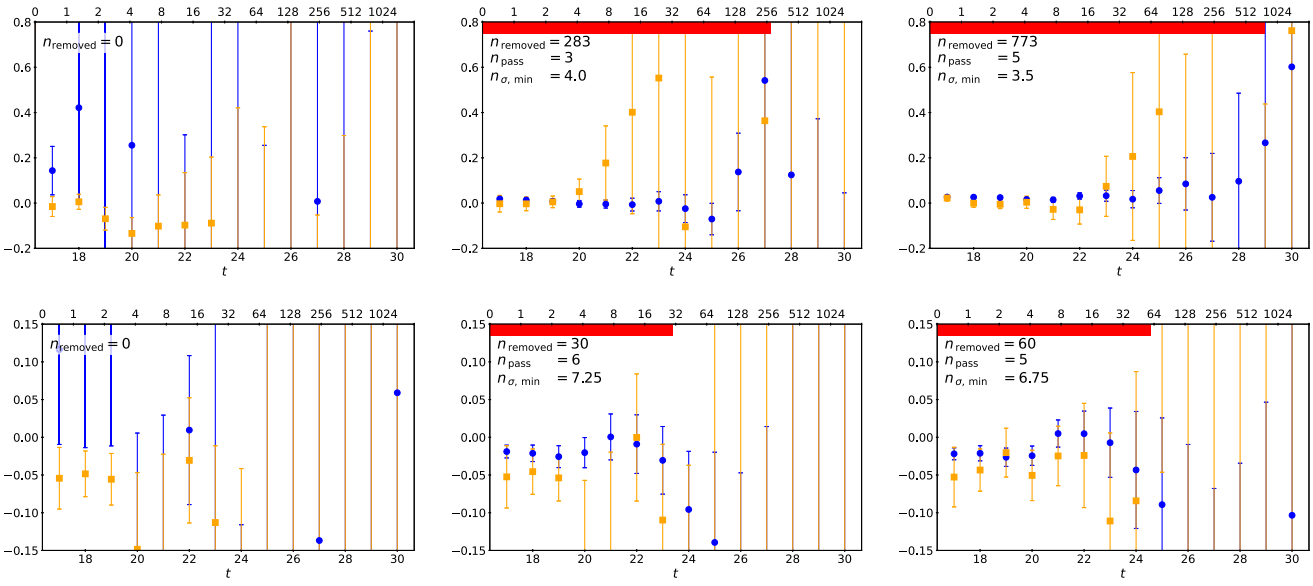


FIG. 4. The effective energy shift $\delta E_\beta(B,t)$ of Eq. (4) for the proton (top) and neutron (bottom). On the left, there are no exceptional configurations removed, the $k_d = 1$-field strength plateau has just resolved in the middle plot and the $k_d = 2$ plateau has just resolved in the right plot. The red bar at the top of the plots indicates the number of configurations removed to achieve the resolution presented. This and the corresponding pass number and $n_{\sigma,\text{min}}$ are also indicated.

A. Nucleons

The effective energy shift $\delta E_\beta(B,t)$ of Eq. (4) for the nucleons are shown in Fig. 4. The proton is the most susceptible of the outer octet baryons to exceptional configurations effects. This is due to the combination of three light quarks in its composition and the doubly represented up quark which feels the background magnetic field more strongly than the down and strange quarks. Due to the difficulty in extracting signal for the proton, we utilize the quality of the $k_d = 1$ plateau and fit in the range $[t_{\text{min}}, t_{\text{max}}] = [20, 25]$. In this case we have removed 773 exceptional configurations of approximately 50 K configurations, a fraction of 1.4%.

Containing three light quarks, the neutron is also affected strongly by exceptional configurations, though the dynamics of the singular up quark reduce its susceptibility compared to the proton. This can be seen in Fig. 4 by comparing the number of configurations that need to be removed to achieve the resolution of the plateau at each field strength.

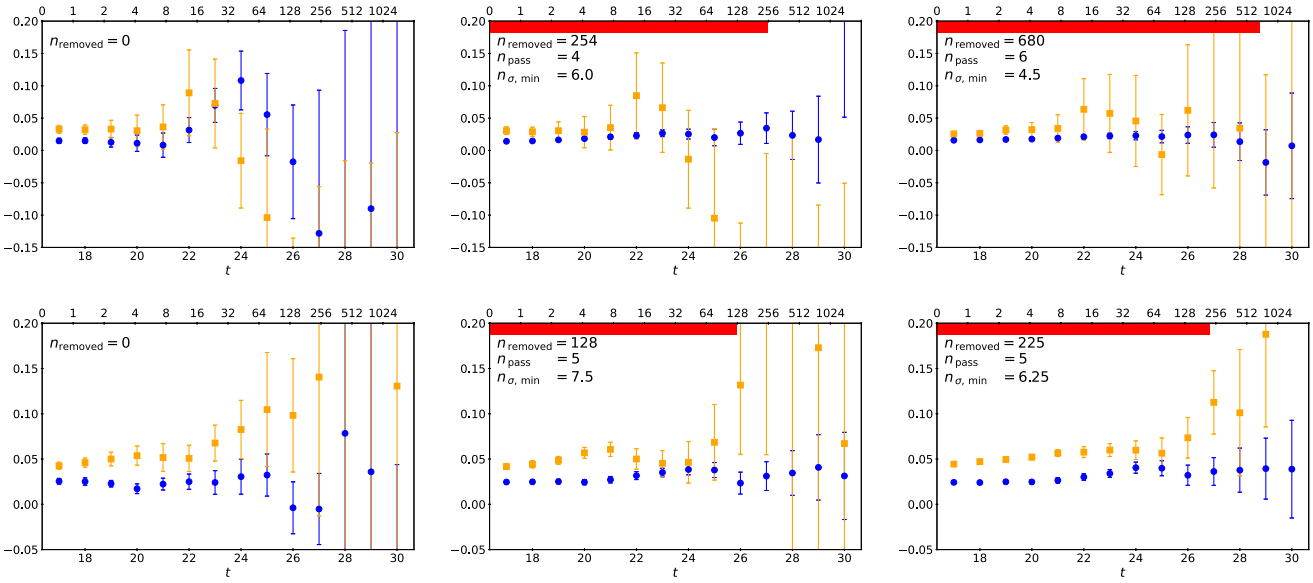


FIG. 5. The effective energy shift $\delta E_\beta(B,t)$ of Eq. (4) for the Σ^+ (top) and Σ^- (bottom). Plots and symbols are as in Fig. 4.

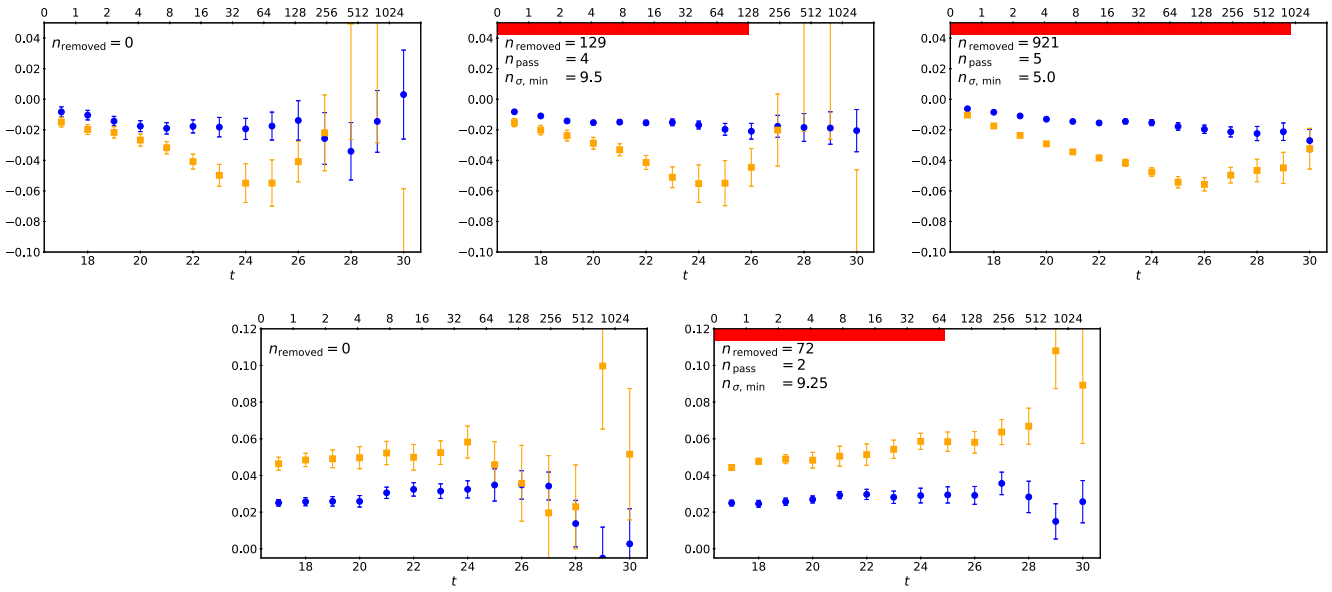


FIG. 6. The effective energy shift $\delta E_\beta(B,t)$ of Eq. (4) for the Ξ^0 (top) and Ξ^- (bottom). Plots and symbols are as in Fig. 4. For the Ξ^- in the bottom row, there is no noticeable jump in the $k_d = 1$ plateau before the $k_d = 2$ plateau is resolved. As such, we simply include the plot with no exceptional configurations removed on the left and the final $k_d = 2$ plateau resolution on the right.

Due to the quickly decaying first field strength plateau, we do not attempt to push the fit later in the case of the neutron, fitting in the range $[t_{\text{min}}, t_{\text{max}}] = [20, 22]$. The neutron requires the removal of only 60 exceptional configurations. While we could leave the algorithm running longer, we have already observed a jump in the quality of the plateau at both field strengths. As such, continuing to remove exceptional configurations would risk removing configurations that are valid signal. Indeed the magnetic polarizability is sensitive to continued configuration removal, tending to increase to larger values. Thus it is important to remove the minimal number of configurations required to resolve the effective energy plateau.

B. Sigma baryons

The plateaus for the Σ baryons are shown in Fig. 5. With the addition of a singular strange quark we see a significant reduction in the susceptibility of the effective energy to exceptional configurations. To emphasize this reduced susceptibility, for each of the hyperons, we will fit the complete untouched set of configurations in addition to the plateaus improved through the removal of exceptional configurations.

As there is still a doubly represented up quark sector in the Σ^+, it is influenced more strongly than the Σ^- in much the same capacity as the relationship between the proton and neutron. This is demonstrated by the difference in number of exceptional configurations removed. For the Σ^+ we remove 680 configurations but only 225 for the Σ^-.

In the full ensemble case, we are only able to fit in the range $[t_{\text{min}}, t_{\text{max}}] = [20, 22]$ for the Σ^+ due to its susceptibility while the absence of an up quark allows fitting of the Σ^- in the range $[t_{\text{min}}, t_{\text{max}}] = [20, 25]$. With the removal of exceptional configurations, we now see good plateau behavior for the Σ^+ and excellent plateau behavior for the Σ^-. The quality of the $k_d = 1$ signal for the Σ^+ allows fitting in the range $[t_{\text{min}}, t_{\text{max}}] = [20, 26]$. Interestingly, the removal of exceptional configurations does not allow for fitting longer for the Σ^- as the $k_d = 2$ signal decays quickly beyond $t = 25$, though it does produce a more precise value.

C. Cascade baryons

The plateaus for the Ξ baryons are shown in Fig. 6. With the strange sector being doubly represented, the plateau

TABLE II. Baryon magnetic polarizability values extracted through fitting the magnetic polarizability energy shift δE_β of Eqs. (4) and (5) over the range $[t_{\text{min}} = 20, t_{\text{max}}]$. In the case of the hyperons, there is sufficient signal available without removing any exceptional configurations to allow fitting. These values are included in the "Untouched" column. The "Exceptional removed" column lists the results from fitting to the rightmost effective energies in Figs. 4–6. The zero-field fit range is $[t_{\text{min}}, t_{\text{max}}] = [20, 30]$. Magnetic polarizability values are in units $\times 10^{-4}$ fm^3.

	Untouched		Exceptional removed	
	t_{max}	β	t_{max}	β
p			25	2.8(16)
n			22	1.7(12)
Σ^+	22	1.7(10)	26	2.17(51)
Σ^-	25	0.42(50)	25	0.41(23)
Ξ^0	25	2.14(32)	29	2.32(20)
Ξ^-	24	0.37(25)	28	0.20(18)

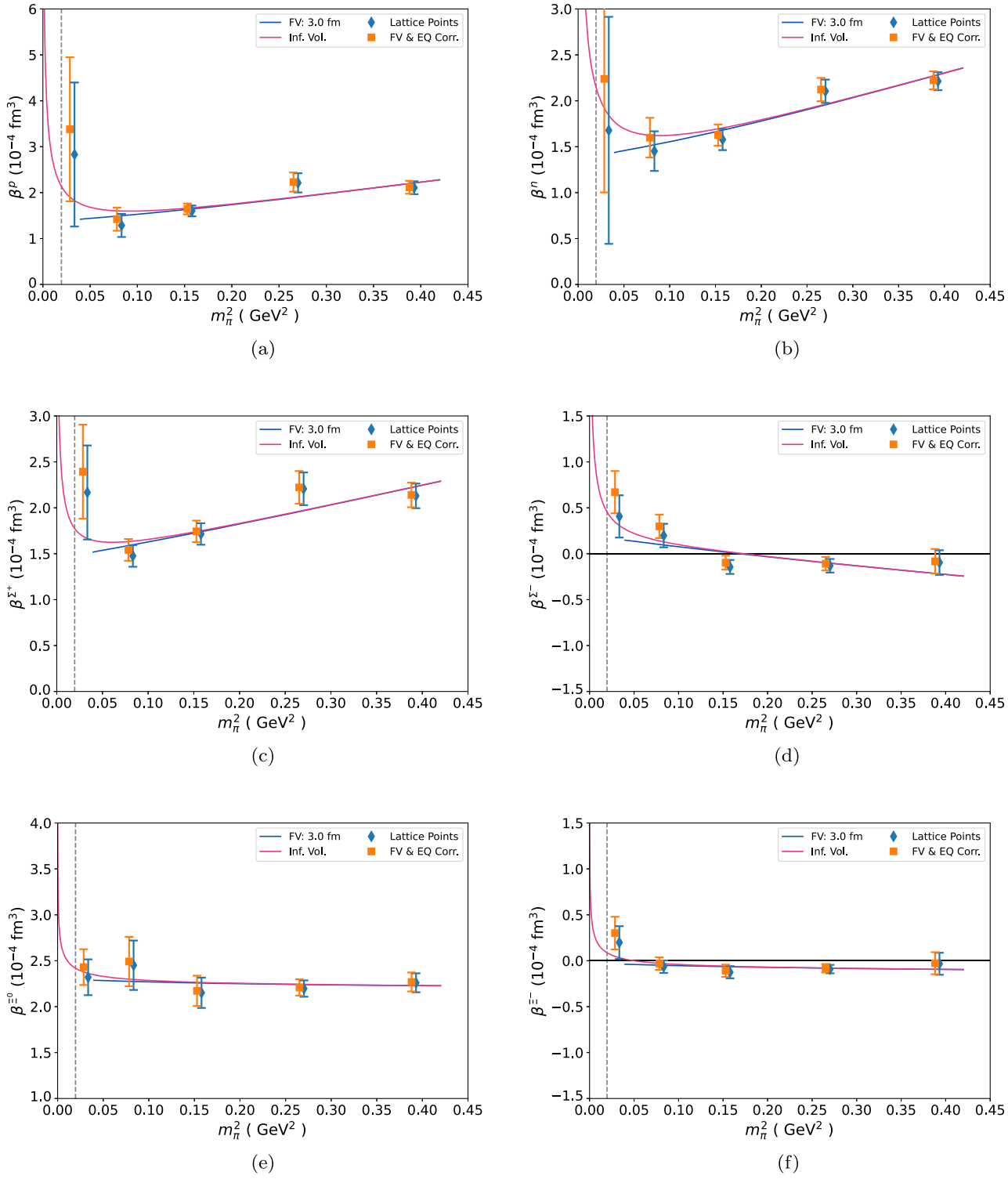


FIG. 7. Chiral extrapolation of the finite-volume and electroquench-corrected (FV EQ Corr.) octet-baryon magnetic polarizabilities to the physical pion mass (vertical dashed line). Extrapolation fits for (a) p, (b) n, (c) Σ^+, (d) Σ^-, (e) Ξ^0, and (f) Ξ^- baryons are presented. Uncorrected lattice points (Lattice Points) are horizontally offset from the corrected points. Extrapolation curves for the 3 fm finite volume for $m_\pi L > 3$ (FV. 3.0 fm) and the infinite-volume extrapolation (Inf. Vol.) are illustrated. The methodology is described in Ref. [5] where the values at the four heaviest masses originate.

profile of the Ξ baryons is cleaner again. The pattern of the u-quark causing increased susceptibility to exceptional configurations continues for the Ξ^0 which requires removal of 921 configurations compared to just 72 for the Ξ^-. We do highlight that while the plateau for the Ξ^0 takes a long time to fully improve, the plateau is extremely good once it does.

The plateau profiles are shown in Fig. 6 but it is important to note here, that the decrease in susceptibility means that the clear jumps in quality of the effective energy are less well defined. This is especially true of the $k_d = 1$ plateau which improves much more gradually, particularly for the Ξ^-, the least susceptible baryon. For this reason, we omit the intermediate plot for the Ξ^- in Fig. 6 and simply include the untouched effective energy and the final effective energy when the $k_d = 2$ plateau is resolved.

The quality of the untouched Ξ^0 plateau allows fitting in the range $[t_{\min}, t_{\max}] = [20, 25]$ as the rapidly increasing $k_d = 2$ plateau prevents extending the fit later without strongly biasing early, potentially contaminated windows. Due to the quality of the Ξ^- plateau, we are very aggressive, terminating the fit at the first sign of noise, hence fitting in the range $[t_{\min}, t_{\max}] = [20, 24]$. With the removal of exceptional configurations, we are able to significantly extend the fit range in both cases. We fit in the range $[t_{\min}, t_{\max}] = [20, 29]$ for the Ξ^0 and $[t_{\min}, t_{\max}] = [20, 28]$ for the Ξ^-.

VI. CHIRAL EXTRAPOLATION

In Ref. [5], we performed a chiral extrapolation to the physical pion mass which includes a correction for the electroquenching of the calculation and an estimate of the finite volume correction. The corrections follow from a consideration of finite-volume partially quenched chiral effective field theory for baryon magnetic polarizabilities [5,31]. The details of the corrections and subsequent extrapolation are given there. Here we include the new light-quark-mass values calculated following the removal of exceptional configurations. Our aim is to provide context for the values determined in the previous section.

The pion mass dependence observed for each baryon is illustrated in Fig. 7. In the figure, we include both the original lattice QCD results and the values obtained after correcting the lattice QCD results for the finite volume and electroquenching. The extrapolation is illustrated for both finite and infinite volume.

We see that, even after the removal of exceptional configurations, the uncertainty for the proton magnetic polarizability at the lightest quark mass remains large. Still, its magnitude is correct and the 1σ uncertainty is in accord with both finite- and infinite-volume extrapolations, largely determined by the four heavier quark-mass points. Perhaps the most important insight is an indication of the level of statistics required to resolve a value with an uncertainty similar to the heavier quark mass considered. Our fourfold increase in statistics over the second-lightest quark mass is not yet sufficient.

Similar results are observed for the neutron. The uncertainties are a little smaller, in accord with a singly represented u quark, and the central values are in better accord with the expectations from the extrapolation curves. It is the presence of three light valence quarks that presents a genuine challenge to precision determinations of the nucleon polarizabilities.

Significant improvement is observed for the hyperons. Even a single strange quark within the Σ^+ is sufficient to tame the unwieldy uncertainty observed for the proton. This time the results sit a little high, just outside the 1σ uncertainty estimate. This trend to sit a little high is also observed for the other charged hyperons. However, the agreement is at the 1σ level. Indeed, for the Σ^-, Ξ^0, and Ξ^-, we observe values obtained following the removal of exceptional configurations that are in accord with the predictions of chiral effective field theory.

The inclusion of values at the lightest quark mass in the chiral fit has minimal impact on the result of the extrapolation to the physical point. In light of the size of the uncertainties and the general agreement observed, this is as one might expect. As a result, we direct the reader to Ref. [5] for our best physical predictions of baryon magnetic polarizabilities, all obtained without the requirement of removing exceptional configurations.

VII. CONCLUSION

Baryon magnetic polarizabilities have been examined for the first time on the $m_\pi = 156$ MeV PACS-CS ensemble [6], closer to the physical point than in any previous work. In pursuing the calculations, an exceptional configuration problem was identified for the nontrivial background-field correlation functions. In an effort to understand the nature and severity of the problem, an algorithm for the systematic identification and removal of the finite-field exceptional configurations has been developed and applied to the PACS-CS ensemble.

Considering the use of a Wilson-type fermion action with additive mass renormalization, the problem appears to be associated with the electroquenching of the sea quarks in the generation of the dynamical-fermion configurations, without regard to the background fields introduced herein. This problem is especially relevant for the nucleons which are most susceptible to such configurations due to their light valence-quark composition. We observed that even a single strange quark can have a strong effect in suppressing the influence of exceptional configurations on baryon correlation functions. Furthermore, the larger electric charge magnitude of the up quark is observed to further enhance the susceptibility of a baryon correlation function to exceptional configuration problems.

Our main focus has been to devise an algorithm to identify and eliminate exceptional configurations from baryon correlation functions at finite background magnetic field. In this way, one can learn about the distribution and

number of electroquenched exceptional configurations and assess the merits of future approaches to the physical quark-mass regime. A key difficulty encountered is to develop a stopping criteria where one can be confident that the minimal number of exceptional configurations are removed from the ensemble. Here, animations of the correlation-function evolution as configurations are removed are particularly helpful, revealing a step change in the resolution of the correlation functions, after which further evolution is slow. Our criteria is to stop exceptional configuration removal immediately after the observed step change.

Using this algorithm to systematically identify and remove exceptional configurations, baryon magnetic polarizabilities are extracted for each of the outer octet baryons containing a doubly represented quark flavor. Our omission of Σ^0 and Λ is due to their mixing in the presence of a background field.

The results are compared with the expectations of partially quenched finite-volume chiral effective field theory. Agreement is observed, typically at the 1σ level, with a trend for the new light-quark-mass results to sit a little high. In light of the larger uncertainties that remain even after exceptional configuration elimination and the general agreement observed with the expectations of chiral effective field theory, the inclusion of these new lattice QCD results have minimal impact on the predictions of the chiral extrapolation at the physical point. To this end, we defer to our previous publication [5] for our best physical predictions of baryon magnetic polarizabilities, obtained without any requirement of removing exceptional configurations.

To determine the magnetic polarizability at light near-physical quark masses, there are several avenues to explore. An obvious approach is to generate new ensembles of dynamical-fermion configurations including interactions between the electrically charged quarks and the background magnetic field. This removes the electroquenching issue and should eliminate the presence of exceptional configurations. However, such an approach loses the important QCD correlations within the correlation-function ratios constructed to resolve the magnetic polarizability. The requirement of an extraordinary increase in statistics is anticipated.

An interim approach could exploit the improved chiral properties of a chiral fermion action, such as the overlap fermion action. In this case, renormalization of the quark mass is multiplicative and this should suppress the issue of exceptional configurations. On the other hand, the trivial-field ensemble forming the foundation of such a calculation is not sampled according to the correct probability distribution and therefore one cannot regard such a calculation as a rigorous first-principles determination. While the overlap action is $\mathcal{O}(100)$ times computationally expensive, correlation functions would maintain the aforementioned QCD correlations. Given that partially quenched chiral effective field theory predicts the electroquenching effects are a relatively small correction to the baryon magnetic polarizabilities, this could be regarded as a reasonable interim approach.

In light of the large number of exceptional configurations encountered, we conclude that electroquenching should follow the path of quenching and not be considered in serious first-principles calculations. While one anticipates future resources enabling the generation of new ensembles of dynamical-fermion configurations including the interactions between the electrically charged quarks and the background magnetic field, one should turn to alternative approaches to the calculation of the magnetic polarizability from first principles.

Here the four-point function approach is demonstrating significant potential [7–11]. Because one works in the zero-field Hilbert space and considers second-order perturbative electromagnetic-field effects, there are no electroquenching issues. It will be important to investigate this approach to understand the challenges of light-quark physics on baryon four-point correlation functions relevant to baryon magnetic polarizabilities.

The results presented herein are founded on the PACS-CS ensembles [6]. The ensembles are created by the PACS-CS Collaboration, Aoki *et al.*, and are available from [32]. The ensembles in question are part of the April 2009 release.

Baryon correlation functions were constructed using the COLA software library, developed at the University of Adelaide [33].

ACKNOWLEDGMENTS

We thank the PACS-CS Collaboration for making their $2+1$-flavor configurations available and the ongoing support of the International Lattice Data Grid (ILDG). W. K. was supported by the Pawsey Supercomputing Centre through the Pawsey Centre for Extreme Scale Readiness (PaCER) program. This work was supported with supercomputing resources provided by the Phoenix HPC service at the University of Adelaide. This research was undertaken with the assistance of resources from the National Computational Infrastructure (NCI), which is supported by the Australian Government. This research is supported by Australian Research Council through Grants No. DP190102215 and No. DP210103706.

DATA AVAILABILITY

The data are not publicly available. The data are available from the authors upon reasonable request.

[1] J. M. M. Hall, D. B. Leinweber, and R. D. Young, Phys. Rev. D **89**, 054511 (2014).
[2] R. Bignell, J. Hall, W. Kamleh, D. Leinweber, and M. Burkardt, Phys. Rev. D **98**, 034504 (2018).
[3] R. Bignell, W. Kamleh, and D. Leinweber, Phys. Rev. D **101**, 094502 (2020).
[4] R. Bignell, W. Kamleh, and D. Leinweber, Phys. Rev. D **100**, 114518 (2019).
[5] T. Kabelitz, R. Bignell, W. Kamleh, and D. Leinweber, Phys. Rev. D **110**, 074514 (2024).
[6] S. Aoki *et al.* (PACS-CS Collaboration), Phys. Rev. D **79**, 034503 (2009).
[7] W. Wilcox and F. X. Lee, Phys. Rev. D **104**, 034506 (2021).
[8] F. X. Lee, A. Alexandru, C. Culver, and W. Wilcox, Phys. Rev. D **108**, 014512 (2023).
[9] F. X. Lee, W. Wilcox, A. Alexandru, and C. Culver, Phys. Rev. D **108**, 054510 (2023).
[10] X.-H. Wang, Z.-L. Zhang, X.-H. Cao, C.-L. Fan, X. Feng, Y.-S. Gao, L.-C. Jin, and C. Liu, Phys. Rev. Lett. **133**, 141901 (2024).
[11] F. X. Lee, W. Wilcox, A. Alexandru, C. Culver, and S. Nadeem, Nucl. Phys. **B1008**, 116701 (2024).
[12] See Supplemental Material at http://link.aps.org/supplemental/10.1103/38db-ml51 for animations showing the evolution of lattice correlation functions as exceptional configurations are eliminated.
[13] T. Kabelitz, W. Kamleh, and D. Leinweber, Phys. Rev. D **111**, 114503 (2025).
[14] G. Martinelli, G. Parisi, R. Petronzio, and F. Rapuano, Phys. Lett. **116B**, 434 (1982).
[15] T. Primer, W. Kamleh, D. Leinweber, and M. Burkardt, Phys. Rev. D **89**, 034508 (2014).
[16] H. Akaike, IEEE Trans. Autom. Control **19**, 716 (1974).
[17] S. Borsanyi *et al.*, Nature (London) **593**, 51 (2021).
[18] F. Di Renzo, in *Proceedings of the 40th International Symposium on Lattice Field Theory* (2024), arXiv:2401.14752.
[19] B. J. Menadue, W. Kamleh, D. B. Leinweber, and M. S. Mahbub, Phys. Rev. Lett. **108**, 112001 (2012).
[20] B. J. Menadue, A study of the $\Lambda(1405)$ in lattice QCD, Ph.D. thesis, Adelaide University, 2018.
[21] D. B. Leinweber, R. M. Woloshyn, and T. Draper, Phys. Rev. D **43**, 1659 (1991).
[22] A. Deshmukh and B. C. Tiburzi, Phys. Rev. D **97**, 014006 (2018).
[23] F. Bruckmann, G. Endrodi, M. Giordano, S. D. Katz, T. G. Kovacs, F. Pittler, and J. Wellnhofer, Phys. Rev. D **96**, 074506 (2017).
[24] E. Chang, W. Detmold, K. Orginos, A. Parreno, M. J. Savage, B. C. Tiburzi, and S. R. Beane (NPLQCD Collaboration), Phys. Rev. D **92**, 114502 (2015).
[25] C. Morningstar and M. J. Peardon, Phys. Rev. D **69**, 054501 (2004).
[26] S. Gusken, Nucl. Phys. B, Proc. Suppl. **17**, 361 (1990).
[27] D. S. Roberts, P. O. Bowman, W. Kamleh, and D. B. Leinweber, Phys. Rev. D **83**, 094504 (2011).
[28] B. C. Tiburzi and S. O. Vayl, Phys. Rev. D **87**, 054507 (2013).
[29] S. Boinepalli, W. Kamleh, D. B. Leinweber, A. G. Williams, and J. M. Zanotti, Phys. Lett. B **616**, 196 (2005).
[30] J. M. Zanotti, S. O. Bilson-Thompson, F. D. R. Bonnet, P. D. Coddington, D. B. Leinweber, A. G. Williams, J. B. Zhang, W. Melnitchouk, and F. X. Lee (CSSM Lattice Collaboration), Phys. Rev. D **65**, 074507 (2002).
[31] J. M. M. Hall, D. B. Leinweber, and R. D. Young, Phys. Rev. D **89**, 054511 (2014).
[32] https://www2.jldg.org/
[33] W. Kamleh, Proc. Sci. LATTICE2022 (**2023**) 339 [arXiv:2302.00850].